JOURNAL OF APPLIED PHYSICS **120**, 095105 (2016)

Charge compensation and electrostatic transferability in three entropy-stabilized oxides: Results from density functional theory calculations

Zs. Rak,[1] C. M. Rost,[1] M. Lim,[1] P. Sarker,[2] C. Toher,[2] S. Curtarolo,[2] J.-P. Maria,[1] and D. W. Brenner[1]

[1]*Department of Materials Science and Engineering, North Carolina State University, Raleigh, North Carolina 27695-7907, USA*

[2]*Department of Mechanical Engineering and Materials Science and Center for Materials Genomics, Duke University, Durham, North Carolina 27708, USA*

(Received 18 July 2016; accepted 20 August 2016; published online 6 September 2016)

Density functional theory calculations were carried out for three entropic rocksalt oxides, $(Mg_{0.1}Co_{0.1}Ni_{0.1}Cu_{0.1}Zn_{0.1})O_{0.5}$, termed J14, and J14 + Li and J14 + Sc, to understand the role of charge neutrality and electronic states on their properties, and to probe whether simple expressions may exist that predict stability. The calculations predict that the average lattice constants of the ternary structures provide good approximations to that of the random structures. For J14, Bader charges are transferable between the binary, ternary, and random structures. For J14 + Sc and J14 + Li, average Bader charges in the entropic structures can be estimated from the ternary compositions. Addition of Sc to J14 reduces the majority of Cu, which show large displacements from ideal lattice sites, along with reduction of a few Co and Ni cations. Addition of Li to J14 reduces the lattice constant, consistent with experiment, and oxidizes some of Co as well as some of Ni and Cu. The Bader charges and spin-resolved density of states (DOS) for Co^{+3} in J14 + Li are very different from Co^{+2}, while for Cu and Ni the Bader charges form continuous distributions and the two DOS are similar for the two oxidation states. Experimental detection of different oxidation states may therefore be challenging for Cu and Ni compared to Co. Based on these results, empirical stability parameters for these entropic oxides may be more complicated than those for non-oxide entropic solids. *© 2016 Author(s). All article content, except where otherwise noted, is licensed under a Creative Commons Attribution (CC BY) license (http://creativecommons.org/licenses/by/4.0/).* [http://dx.doi.org/10.1063/1.4962135]

I. INTRODUCTION AND MOTIVATION

Multi-component high entropy alloys (MHEAs), defined as four or more components in roughly equi-atomic concentrations randomly arranged on a single phase crystalline lattice, are of current interest due to both their potential for unique thermodynamic phase stability[1–3] and for their potential applications.[4–10] Up until recently, this class of high entropy material was restricted to metals and refractory ceramics[11–14] with relatively simple crystal structures within which all of the lattice sites are part of the entropic phase. In a recent set of experiments, Rost *et al*. demonstrated a new class of material in which entropy drives the free energy landscape, an entropy-stabilized oxide (ESO).[15] The first system reported, which was termed the J14 composition, has a rocksalt structure with one of the face-centered cubic (fcc) sublattices containing oxygen anions, and the other sublattice containing randomly arranged Mg, Co, Ni, Cu, and Zn cations in equi-atomic proportions. In addition to being an oxide, this system is a unique combination of an ordered and a disordered sublattice together within a single high entropy phase.

Following up on the results of Rost *et al.*,[15] Berardan *et al*. reported that the single-phase, entropic rocksalt structure of J14 is maintained with the addition of Li and Li co-incorporated with Ga as substitutional (rather than interstitial) defects.[16,17] The former is commonly associated with a +1 formal charge state, and so the authors suggest charge compensation involving oxidation of Co^{+2} to Co^{+3} and/or creation of O vacancies. They report that the addition of Ga without Li resulted in formation of a $CuGa_2O_4$ phase, which they suggest may be due, in part, to the system being unable to accommodate the Ga^{+3} formal charge state. However, the authors suggest that the accommodation of Ga when paired with Li occurs because of charge compensation between the Li-Ga pairs, which does not require formation of O vacancies. Berardan *et al*. also measured the electrical resistivity of the J14 and J14 + Li materials. For the former, they report semiconducting behavior with a band gap of ~0.8 eV, which decreases to ~0.35 eV with addition of an equi-atomic amount of Li. They also report a decrease in the J14 + Li lattice constant that is linear with increasing mole fraction of Li.

Berardan *et al*. have also successfully incorporated Na and K into the J14 material, with charge compensation thought to occur through O vacancy formation.[17] The Maria research group has also shown that the entropic rocksalt structure is maintained for the addition of other oxide-forming elements, including Sc, Cr, Sb, Ge, Sn, and Ca.[18] Details of the experiments with Sc (a cation commonly associated with a +3 charge formal state) are discussed below.

There are clearly tremendous possibilities for designing materials of this type with potentially interesting and unique properties and applications.[15–17]

Zhang *et al.*[3] demonstrated that the stability of non-oxide MHEAs can be reasonably predicted based on two empirical parameters that can be derived from the component elements, a measure of the differences in atomic radii and the mixing enthalpy for a solid solution. In addition, to enhance the free energy of the MHEAs the entropy of mixing should be maximized, which occurs for equi-molar concentrations.[3] A number of other parameters have also been introduced for predicting the stability and crystal structure of non-oxide MHEAs.[1] These additional parameters are based on quantities such as the electro-negativities and melting points of the pure components, the enthalpy of formation and entropy of mixing for the binary compounds,[2] and component electron densities and valence electron concentrations.[1] These and similar criteria have also been combined with high-throughput first principles calculations to better understand their origins and to improve predictions for a wider range of possible compositions.[19,20] The relatively large number of known non-oxide MHEAs revealed these criteria and allowed predictive methods to be developed and validated by comparison to experiment.[2,3]

The J14 composition was chosen to satisfy a number of criteria that included similar ionic radii and formal (i.e., integer) charge states, not all of the lowest energy structures for the binary compositions are rocksalt, and there is limited immiscibility for some of the binary pairs (e.g., MgO-ZnO).[15] The former two criteria are similar to the traditional Pauling model that relates ion radii and charge to oxide structure and are also similar to those used to incorporate lattice strain effects into the prediction of non-oxide MHEA compositions.[1,3] The latter two criteria for the oxides were chosen to help demonstrate true entropic stabilization.

The successful addition of elements other than those in the J14 composition that require charge compensation to satisfy charge neutrality suggests that other criteria may be important for predicting stability of these materials. Plotted in Figure 1 are effective cation radii for +1, +2, and +3 formal charges as a function of atomic number for the species in the J14 composition, as well as for Sc and Li.[21] The solid horizontal line is the average radius of the J14 elements. The two horizontal dashed lines define a region containing the radii for the J14 elements in +2 charge states; these lines are plus and minus 9% of the J14 average. Li^{+1} and Sc^{+3} both fall close to the average J14 value, while the radius associated with the Sc^{+1} charge state is much larger than this range. Although an effective ionic radius could not be located for Sc^{+2}, based on the large difference between the +1 and +3 radii, this radius would likely be well out of the regime defined by the dashed lines. Note also that Cu has +1 and +2 formal charge states with radii that fall within this range. These data suggest a possible charge/strain compensation effect for the two J14 + Sc and J14 + Li compositions. For the latter, Sc^{+3} could fit in the lattice, but would require reduction of one or more of the J14 elements for charge neutrality. With both +1 and +2 oxidation states in this range of radii, Cu is a potential candidate. Similarly, the effective ionic radius for Li^{+1} fits within the radius range but would require oxidation of one or more of the J14 elements. As measured by Berardan *et al.*,[16,17] oxidation of Co^{+2} to Co^{+3} is a viable mechanism, but based on Figure 1 the radius of Co^{+3} ions is below the radius range defined by the horizontal dashed line. We note also that the radii for Ni^{+3} and Cu^{+3} are below this regime. The Density Functional Theory (DFT) results discussed below indicate that Ni and Cu are oxidized in addition to Co with the introduction of Li into the J14 composition.

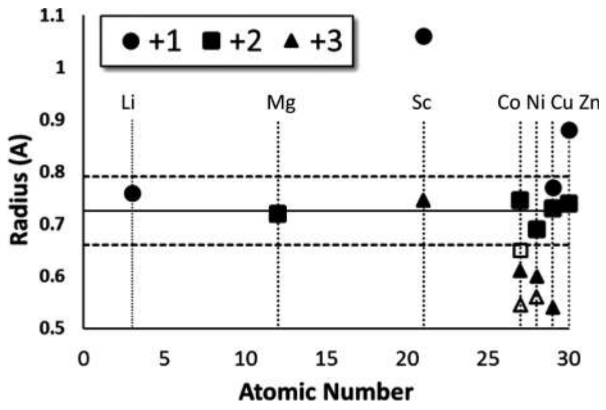

FIG. 1. Effective ionic radii as a function of atomic number for the J14 elements as well as Li and Sc. The high and low spin states are indicated by closed and open symbols, respectively.

The heat of mixing parameter derived from pairs of components, which was successfully used to help predict whether a collection of non-oxide components will form a MHEA, was taken as a sum of the regular melt-interaction parameters for pairs of components weighted by their atomic percent.[3] Whether a similar expression for combining oxide formers may exist for random oxides will likely depend on whether the contributions to Coulombic bonding in the binary or ternary oxides for the individual components transfer to the random oxide. This in turn will depend on whether the ion charges in the binary compositions (which in the true systems may not have simple integer values) are maintained in the high entropy mixture or if they equilibrate through charge transfer either locally through second-neighbor interactions or globally throughout the system. As noted above, charge state and radius (and hence lattice strain) are also closely related, which potentially complicates the derivation of a single parameter based on ionic radii. Furthermore, the current dearth of data related to the formation of entropic oxides hinders the empirical development of reliable parameters for stability.

With these and similar issues in mind, we have carried out Density Functional Theory (DFT) calculations on the J14, J14 + Sc, and J14 + Li compositions in a rocksalt structure for both binary and equi-atomic ternary compositions, as well as for relatively large systems that represent supercells of the equi-atomic high-entropy rocksalt structures. The calculations suggest that the J14 composition is relatively well behaved in terms of the transferability of Bader charges and lattice constants between the binary, ternary, and random structures. When Sc and Li are added, however, the requirement of charge neutrality results in the reduction and oxidation, respectively, of other cations in the random structure such that the average Bader charge for each element is not necessarily transferable across compositions. In addition, the radii associated with the altered oxidation states do not necessarily fall within the range of effective ionic radii defined by the ions in the J14 composition, potentially complicating expressions that rely on similar radii to predict stability of the entropic rocksalt structure. As discussed in detail below, these changes in charge state can also add disorder to the system in terms of both Bader charges associated with the atoms as well as in displacements of atoms from their ideal lattice sites.

II. SYNTHESIS OF THE J14 + Sc COMPOSITION

Berardan *et al*. report an inability to incorporate +3 ions into J14,[16,17] in contrast to recent work by Rost.[18] Because details of the Sc incorporation have not previously appeared in the literature, we include a brief description of the experimental procedure in this section. Further details can be found elsewhere.[18]

Composition J14 + Sc (also termed J30[18]) was synthesized by combining ∼18.337 mol. % of MgO (Alfa Aesar 99.99%), NiO (Sigma Aldrich 99%), CuO (Alfa Aesar 99.9%), CoO (Alfa Aesar 99%), ZnO (Alfa Aesar 99.9%), and ∼8.335 mol. % Sc_2O_3 (Sigma Aldrich, 99.9%). Massed powders were mixed and shaker milled using yttrium-stabilized zirconia media for 1 h, then pressed into 1.27 cm pellets using 8000 lbs of uniaxial force and reacted at 1000 °C in air for 12 h. Bulk J30 exhibits two structural phases as evidenced by x-ray diffraction: rocksalt and scandia (spacegroup: Ia-3).[15] Scandium was successfully incorporated into J14 though pulsed laser deposition (PLD). Thin films were grown on (100) MgO substrates using a 248 nm KrF excimer laser. Substrates are cleaned using a solvent rinse sequence of acetone, isopropanol, and methanol followed by a 10 min UVO treatment. Deposition temperature was held at 400 °C; the target-substrate distance and O_2 pressure remained consistent at 5 cm and 50 mTorr, respectively. X-ray diffraction measurements were done on both bulk and thin film samples using a PANalytical Empyrean diffractometer operated at 45 kV–40mA.

Shown in Fig. 2(a) is a 2θ-ω scan about the (200) MgO peak with a film peak to the left of the substrate, indicating a larger out-of-plane lattice parameter, consistent with rocksalt. Additional symmetric and skewsymmetric scans covering angular ranges for scandia and spinel reflections were conducted to explore the possibility of additional epitaxial phases. No evidence was found; thus, we conclude that to the limits of a laboratory x-ray instrument, these samples are single phase and exhibit the rocksalt structure. Furthermore, in-plane scans showed that the films are pseudomorphic to the MgO substrate. The presence of well-defined Pendellösung fringes is a result of interference between incident and diffracted waves within the film.[22,23] These are typically an indicator of a high crystal quality thin film with a smooth, abrupt hetero-epitaxial interface. A comparison between film and substrate of the (002) rocking curves is shown in Fig. 2(b).

Energy-dispersive spectroscopy (EDS) is used as a preliminary, qualitative means to check for gross chemical clustering. Thin film samples were prepared for measurements by coating each with a ∼15 nm thick layer of Pt metal to negate charging. EDS was done using an FEI Quanta 3D FEG SEM set to 20 kV and 8 nA. Ten maps were collected per cation species encompassing an area of 3600 μm^2. Results shown in Fig. 3 suggest all expected cations to be present, and there is no indication of significant chemical clustering.

III. DENSITY FUNCTIONAL THEORY CALCULATIONS

The DFT calculations were performed using the projector augmented wave (PAW)[24,25] method as implemented in the Vienna *Ab initio* Simulation Package (VASP).[25–27] The generalized gradient approximation as parameterized by Perdew *et al*. was used for the exchange-correlation potential,[28] and the standard PAW potentials, supplied with the VASP 4.6 package, were also used. For these potentials, the semi-core p-states of Ni and Cu are treated as valence states while for Co and Zn the semi-core states are kept frozen. The number (and configuration) of valence electrons considered in the calculations are 3 ($1s^22s^1$) for Li, 8 ($2p^63s^2$) for Mg, 11 ($3s^23p^64s^23d^1$) for Sc, 9 ($3d^74s^2$) for Co, 16 ($3p^63d^94s^1$) for Ni, 17 ($3p^63d^{10}4s^1$) for Cu, 12 ($3d^{10}4s^2$) for Zn, and 6 ($1s^22p^4$) for O. To better describe the behavior of

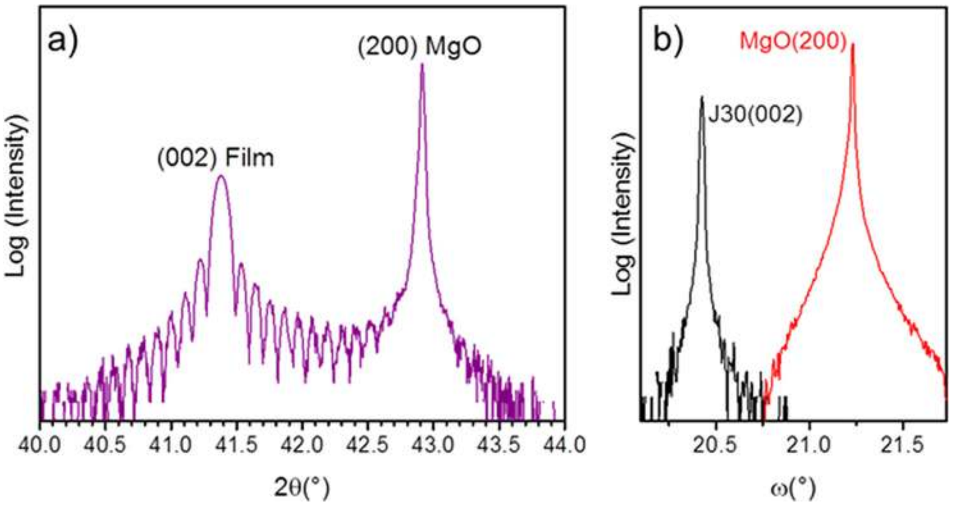

FIG. 2. Diffraction data for the J14 + Sc composition. (a) 2θ-ω scan around the (200) MgO substrate peak. The (200) J30 film peak is located to the left of the substrate, at lower 2θ, indicating a larger out of-plane d-spacing calculated to be 4.31 Å. (b) Omega rocking curves of the (002) peak of the J30 film compared to the MgO substrate. The rocking curves were collected at the optimized 2θ positions for the film and substrate, respectively. The substrate and film have full-width-half-maximum values of 0.013° and 0.018°, respectively.

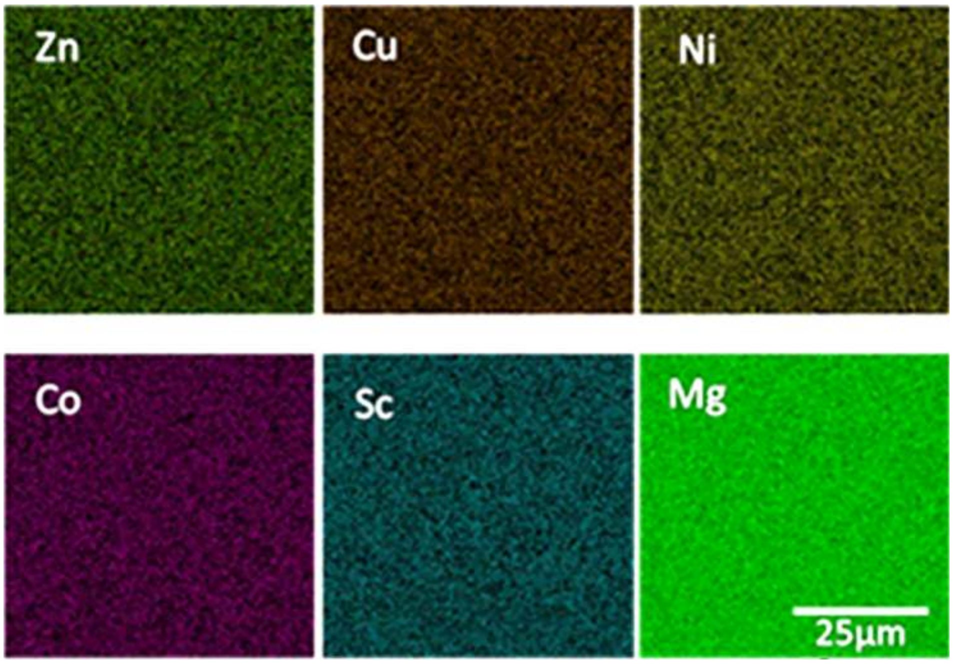

FIG. 3. EDS map of J30 rocksalt showing the spatial distribution of constituent cations within one fcc sublattice. Observation of each map suggests an overall uniform cation distribution throughout the sampling area with minimal cation clustering. Mg appears to be brighter because the system is detecting the MgO substrate in addition to the film.

the localized 3*d* electrons in the row four elements, the orbital-dependent, Coulomb potential was included in the calculations using the DFT+ Hubbard *U* formalism in the simplified, rotationally invariant approach introduced by Dudarev *et al*.[29] The U values used were 2.9, 5, 5.1, 4.5, and 7.5 for Sc, Co, Ni, Cu, and Zn, respectively.[30] A cut-off energy for the plane wave basis was set to 560 eV, and convergence was assumed when the energy difference between two consecutive self-consistent cycles was less than 10^{-4} eV. For small binary and mixed oxide systems (8 atoms/cell, NaCl structure), the Brillouin-zone was sampled by a Γ-centered, $16 \times 16 \times 16$ k-mesh, while only the Γ point was used for the larger cells. To accurately reproduce the correct total core charge for Bader analysis,[31] the fast-Fourier transform grid was increased to (228, 228, 228). Volume optimizations were carried out by fitting the total energies for different volumes to the Birch-Murnaghan equation of state.

To model random oxides, a 480 atom rocksalt supercell was generated with size $3 \times 4 \times 5$ unit cells containing 8 atoms each. The cation sublattice was populated using the special quasi-random structure algorithm with equal numbers of each cation type.[32] Therefore, the J14 composition contained 48 of each of the five cation types, while the J14 + Sc and J14 + Li compositions had 40 of each cation type. Two structures were simulated, one where atoms are restricted to the ideal rocksalt lattice with the lattice constant optimized with respect to energy, and structures in which the atoms and supercell shape and dimension were allowed to relax from the ideal rocksalt values. Experimentally, the entropic rocksalt oxide only becomes the thermodynamically stable phase at elevated temperatures,[15,18] and therefore, the relaxed structures do not likely represent the lowest energy configuration. Instead, the calculations are intended to probe possible deviation of the ions from ideal sites due to lattice strain, and any effects such strains may have on the electronic structure of the material.

IV. RESULTS

Table I is a summary of all of the DFT results. Included are the calculated minimum-energy lattice constants and the Bader charges for the binary and ternary oxides in an ideal rocksalt structure, as well as averaged data for the ternary systems and for the large ideal and relaxed random systems.

A. J14

For binary combinations of elements possible within formulation J14, each calculated lattice constant is less than 0.4% from the average of their binary structures, consistent with the discussion in Section I. In addition, the average lattice constant for the ternary compositions and the lattice constants for the ideal and relaxed large random structures are within 0.16%, 0.29%, and 0.14% of the average of the binary compositions, respectively.

The Bader charges for the binary oxides are not uniform between elements, and each of the Bader charges for the ternary compositions of the J14 cations remain relatively unchanged from their respective binary compositions. The largest percent changes, for example, are for the J14 elements paired with Mg, which are only 6.1%, 2.8%, 2.7%, and 2.1% for Cu, Ni, Zn, and Co, respectively. Furthermore, the Bader charges from the binary, the averages from the ternary systems, and the averages for both random systems are all close, as apparent from the data in the table. The largest deviation is for Cu, which shows a difference of 3.9% between the ideal binary and the relaxed J14 structure. The similar lattice constants and Bader charges suggest that for the J14 elements the ionic bonding does not change significantly from the binary to the ternary to the random compositions.

Plotted in Figures 4(a) and 4(b) are Bader charge distributions for the binary oxides in the table and for the 480 atom J14 supercell, respectively, both in ideal rocksalt lattices. Plotted in Figure 4(c) is the same data for the random

TABLE I. Summary of the DFT results.

		Bader charges								
System	Lattice constant (A)	Li	Mg	Sc	Co	Ni	Cu	Zn	O	O
LiO	4.129	0.88								
MgO	4.259		1.70						−1.70	x
ScO	4.558			1.64					−1.64	x
CoO	4.253				1.27				−1.27	x
NiO	4.242					1.24			−1.24	x
CuO	4.257						1.04		−1.04	x
ZnO	4.214							1.22	−1.22	x
$LiMgO_2$	4.204	0.88	1.71						−1.16	−1.43
$LiCoO_2$	4.114	0.88			1.37				−1.06	−1.19
$LiNiO_2$	4.079	0.87				1.33			−1.07	−1.14
$LiCuO_2$	4.079	0.88					1.14		−1.03	−0.99
$LiZnO_2$	4.133	0.88						1.25	−1.02	−1.11
$MgScO_2$	4.484		1.68	1.72					−1.72	−1.68
$MgCoO_2$	4.280		1.71		1.24				−1.54	−1.41
$MgNiO_2$	4.246		1.71			1.21			−1.54	−1.39
$MgCuO_2$	4.252		1.72				0.98		−1.45	−1.24
$MgZnO_2$	4.234		1.71					1.18	−1.53	−1.37
$ScCoO_2$	4.425			2.01	0.78				−1.44	−1.36
$ScNiO_2$	4.428			1.99		0.77			−1.42	−1.34
$ScCuO_2$	4.447			2.04			0.67		−1.42	−1.29
$ScZnO_2$	4.496			1.86				0.96	−1.47	−1.34
$CoNiO_2$	4.270				1.26	1.24			−1.25	−1.25
$CoCuO_2$	4.264				1.30		1.03		−1.21	−1.12
$CoZnO_2$	4.262				1.28			1.21	−1.26	−1.23
$NiCuO_2$	4.247					1.26	1.04		−1.18	−1.11
$NiZnO_2$	4.228					1.25		1.21	−1.24	−1.22
$CuZnO_2$	4.233						1.03	1.22	−1.10	−1.15
J14 Ternary ave.	4.252	x	1.71	x	1.27	1.24	1.02	1.21	−1.29	
J14 Averages, ideal	4.257	x	1.70	x	1.26	1.20	1.09	1.18	−1.29	
J14 Ave., relaxed	4.251	x	1.7	x	1.26	1.23	1.08	1.21	−1.29	
J14 + Sc Ternary ave.	4.320	x	1.71	1.92	1.17	1.14	0.95	1.16	−1.34	
J14 + Sc Ave., Ideal	4.357	x	1.69	2.02	1.20	1.12	0.81	1.14	−1.33	
J14 + Sc Ave. relaxed	4.343	x	1.70	2.05	1.19	1.18	0.66	1.20	−1.33	
J14 + Li Ternary ave.	4.208	0.88	1.71	x	1.29	1.26	1.04	1.22	−1.23	
J14 + Li Ave., ideal	4.204	0.88	1.69	x	1.31	1.21	1.12	1.19	−1.24	
J14 + Li Ave., relaxed	4.212	0.88	1.7	x	1.33	1.25	1.15	1.21	−1.26	

J14 composition after relaxation. The oxygen ions in the large systems display a relatively continuous distribution of Bader charges that has an average value that matches the average of the ternary compositions (see the table). For each of the cations, the Bader charges spread into individual distributions that are centered very close to the charges for their respective binary compositions. The largest spread in the random structure is for Cu, which ranges from 1.02 (0.99) to 1.16 (1.15) in the ideal (relaxed) structure compared to the range of 0.98–1.04 for Cu in the ternary compositions. The smallest spread is for Mg, which ranges from 1.69 to 1.71. Hence for the entropic J14 composition, the set of charges on the oxygen sublattice appear to equilibrate to a continuous distribution, while the charge distributions on the cation sublattice reflect those of the individual cations with the degree of broadening depending on the cation type.

Plotted in Figure 5 are the spin resolved total density of states (DOS) and the Cu-3*d* partial DOS (PDOS) near the Fermi level for the large system both in the ideal rocksalt structure (Fig. 5(a)) and after relaxation (Fig. 5(b)). The most significant difference between the DOS of the relaxed and unrelaxed systems is the presence of the peak located at the Fermi level of the unrelaxed system. This peak is also present in the Cu-3*d* PDOS and it originates, most likely, from the two degenerate e_g orbitals of Cu^{+2} that are occupied by 3 electrons. Upon relaxation, the degeneracy is removed and a gap of ∼0.5 eV opens up in the electronic structure of the J14 system. Given the well-known band gap problem of DFT, this is reasonably close to the value of ∼0.8 eV reported by Berardan *et al.*[16] Plotted in Figure 6 are the average atom displacements for the three large systems as a function of element type. For J14 (open bars), the displacements from the ideal rocksalt lattice after relaxation are relatively small and uniform for each cation type. There is a slightly larger average displacement for the oxygen anions. Hence, the splitting of the copper *d* states near the Fermi level does not appear to result in a significant displacement of the Cu cations away from the ideal lattice sites. There is,

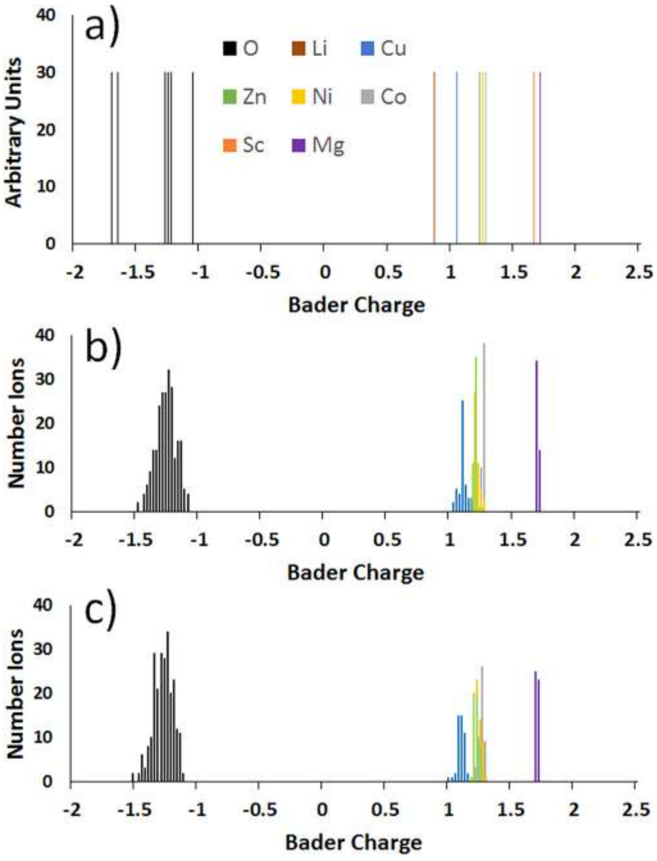

FIG. 4. Bader charge distributions from the DFT calculations. (a) From the binary compositions in the unrelaxed, ideal rock salt structure. (b) From the 480 atom randomized J14 composition in an ideal rock salt structure. (c) Same system as (b) after relaxation.

however, some experimental evidence for a Jahn-Teller distortion of the O atoms that is associated with the charge states of Cu.[18] The data presented here are currently being thoroughly analyzed in conjunction with those experimental results.

B. J14 + Sc

Plotted in Figure 7 are charge distributions for the J14 + Sc system, which together with compositions containing Sc in Table I shows different behaviors compared to the J14 composition alone. For the binary oxides, ScO has the largest lattice constant, and Sc has the largest Bader charge of the fourth row elements, consistent with the discussion above related to the data in Figure 1. When paired with Sc in a ternary composition, all of the other cations are reduced, while Sc is oxidized. Co, Ni, and Cu all lose over 36% of their Bader charge, while Zn loses 21% of its charge. For the former three elements, the charge on Sc increases 22.5%, 21.2%, and 24.3%, while for Zn it increases 13.3%. The smallest effect occurs when Sc is paired with Mg; in this case, the Sc charge increases only 4.7% while the charge on Mg decreases by 1.6%.

Based on the relatively large changes in Bader charges from the binary to ternary compositions when J14 elements are paired with Sc, the ionic bonding properties of the J14 + Sc random alloy may not be accurately predicted from the binary structures alone. However, the average charges from the ternary compositions are reasonably transferable to the random structure except for Cu, and to a lesser degree for Sc. For Mg, Co, Ni, Zn, and O, for example, the changes in Bader charge from the average of the ternary structures to the random structure are 2.3% or less. In contrast, for Cu and Sc, this change is 14.6% and 5.1%, respectively.

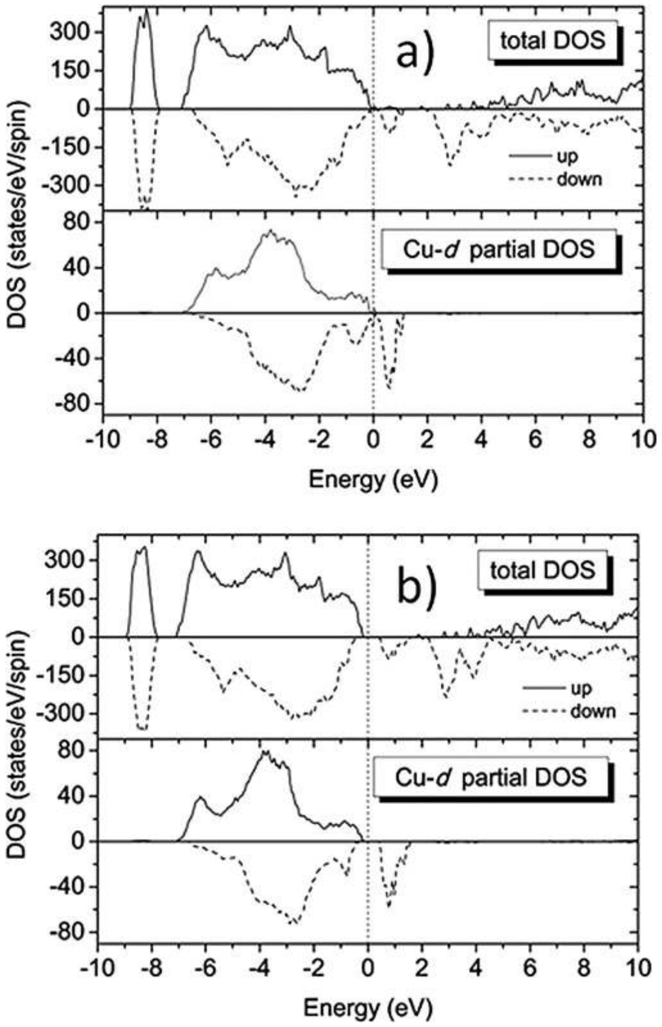

FIG. 5. Spin resolved DOS from the DFT calculations for the (a) ideal and (b) relaxed J14 structures. The top plots are the total DOS, while the bottom plots in each panel are the DOS for Cu atoms only.

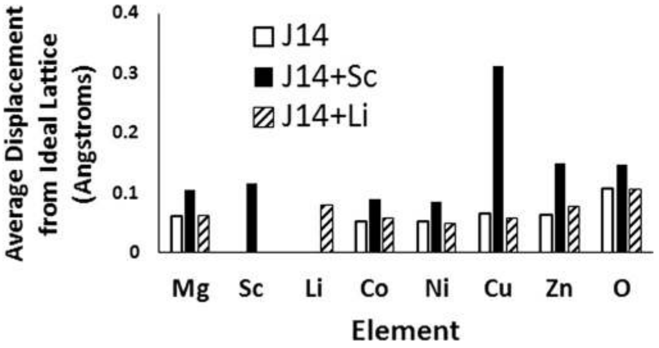

FIG. 6. Average displacement from the ideal rock salt lattice sites for the three large random systems (denoted by the shading on the bars) as a function of element type.

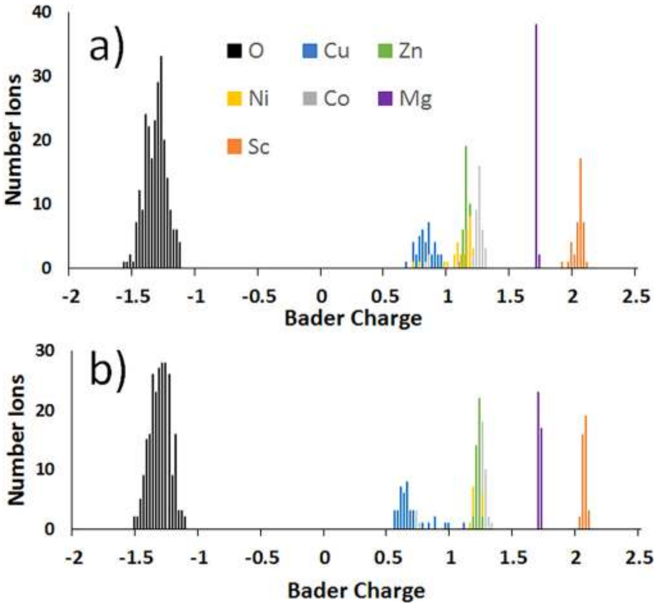

FIG. 7. Bader charge distributions from the DFT calculations. (a) From the 480 atom randomized J14 + Sc composition on an ideal rock salt lattice. (b) Same system as (a) after relaxation.

Additional information related to Bader charge transferability is also apparent by comparing Figures 4 and 7. The distribution of Bader charges for the oxygen ions in the J14 and J14 + Sc compositions remains similar both in where they are centered (a difference of about 3%) as well as in their width and shape. Furthermore, in both the J14 and J14 + Sc compositions, the average oxygen Bader charges are transferable between their respective ternary and random structures. In addition to lowering the average charge of the J14 ions with the addition of Sc, with the exception of Mg, the charge distributions are all broadened over the J14 composition without Sc. Given that Sc comprises only one sixth of the cations, this is to be expected because only a limited number of other cations will have Sc as a second neighbor, provided that the charge transfer effect is local. We note, however, that this broadening is most pronounced for Cu, and after relaxation, the average charges on the Cu atoms shift to lower values and the distribution broadens.

To further quantify and understand the results based on the Bader charges, formal oxidation states were determined for each cation by analyzing their spin magnetic moments. Plotted in Figure 8 are distributions of Bader charges for the Co, Ni, and Cu cations in the relaxed structure. The shading of each bar denotes the number of cations with a given charge state (as determined from the magnetic moments) for the Bader charge. Based on this analysis, four Co cations and one Ni cation were reduced from a formal charge of +2 to +1. Of the 40 Cu cations, 29 were identified as having been reduced to a +1 formal charge and three retained their +2 formal change. A definitive formal charge of +1 or +2 could not be assigned for the remaining eight of the Cu cations. (This can be considered somewhere between the two formal integer charges.) Each of the reduced cations show a concomitant reduction in their Bader charges. The number of Co, Ni, and Cu ions in various oxidation and spin states for the three entropy stabilized systems under investigation are listed in Table II.

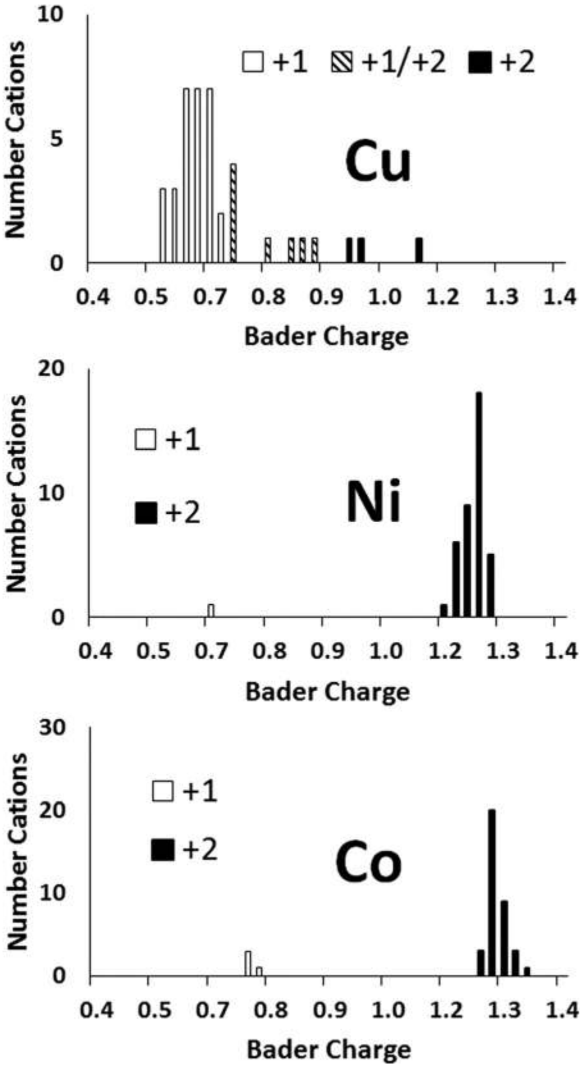

FIG. 8. Bader charge distributions for Cu, Ni, and Co in the J14 + Sc relaxed system. The coloring of each bar denotes the number of cations with a given charge state as determined from the magnetic spins.

The system was also examined to determine if there is a correlation between the reduction of the Cu ions and their

TABLE II. The number of Co, Ni, and Cu ions in various oxidation states with corresponding *d*-electron configurations and spin states for the three entropy stabilized oxides.

			J14	J14 + Sc	J14 + Li
Co	1+	(d^8)	…	4-HS	…
	2+	(d^7)	48-HS	36-HS	30-HS
	3+	(d^6)	…	…	7-HS; 3-IS
Ni	1+	(d^9)	…	1	…
	2+	(d^8)	48-HS	39-HS	30-HS
	3+	(d^7)	…	…	10-HS
Cu	1+	(d^{10})	…	29	…
	1+/2+	($d^{9/10}$)	…	8	…
	2+	(d^9)	48	3	18
	2+/3+	($d^{8/9}$)	…	…	5
	3+	(d^8)	…	…	17-HS/LS

proximity to Sc ions. Most of the reduced Cu ions have at least one next-nearest neighbor Sc (all of the near neighbors are O); however, there are also reduced Cu ions with no Sc next-nearest neighbors. In addition, out of the three Cu ions that retained their +2 charge, one has no Sc next-nearest neighbor, one has one Sc next-nearest neighbor, and one has two Sc next-nearest neighbors. Hence, there does not appear to be an obvious correlation between proximity to Sc and the reduction of Cu ions.

Shown in Figure 6 as the filled bars are the average displacements in J14 + Sc for each element. For this system, the average Cu displacement is 2–3 times larger than the other elements in any of the systems studied. Plotted in Figure 9 is the Bader charge for each of the Cu cations in the J14 + Sc system as a function of displacement of the Cu cation from its ideal lattice site. The formal charges are indicated by the shading. Eight of the 40 Cu atoms show relatively large displacements that are greater than 0.5 Å, each with a Bader charge of between 0.5 and 0.6 and a +2 formal charge. The remaining reduced Cu cations as well as the Cu cations with a +2 charge state or whose charge state could not be determined show much smaller displacements. In contrast, the Sc retains its relatively large charge and remains relatively close to the ideal lattice sites. Hence, we conclude that the addition of Sc adds to the structural disorder in the system by reducing a majority of the Cu cations, and some fraction of which then move from their ideal lattice sites.

C. J14 + Li

Berardan *et al*. report a decrease in the J14 + Li lattice constant that is linear with increasing mole fraction of Li.[16] Noting that the crystal ionic radius of Li is larger than the average radii for the J14 elements, they attribute the decrease in lattice constant with the oxidation of Co^{+2} to Co^{+3}, and to the formation of O defects.[16,17] The former is supported by X-ray Photoelectron Spectroscopy (XPS) data, which indicate oxidation of some of Co, although not enough to fully compensate the charge state of all of the added Li. For the compositions containing Li, the DFT calculations (see Table I) yield lattice constants for the binary, all of the ternary compositions, and the J14 + Li random structure that are all smaller than those for the J14 elements alone. The lattice constant for the J14 random structure in the ideal rocksalt lattice goes from 4.257 to 4.204 Å with addition of an equi-atomic concentration of Li, a decrease of 0.053 Å. The corresponding decrease in lattice constant for the relaxed systems is 0.045 Å. The experimental data[16] indicate a change in lattice constant of 4.2277–4.1712 Å, a difference of 0.056 Å. Hence, we conclude that at least for one data point (the equi-atomic concentration) the change in lattice constant observed experimentally is reproduced reasonably well from these DFT calculations without invoking oxygen vacancies.

Based on the data in Table I, the average Bader charges on Li and Mg remain constant for the binary, ternary, and random compositions. Comparing the J14 and J14 + Li random structures, it appears that charge compensation for addition of Li largely occurs through the oxidation of Co, Cu, and Ni. Plotted in Figures 10(a) and 10(b) are the Bader charge distributions for the random J14 + Li composition in an ideal rocksalt structure and in the same structure that was allowed to relax in atom position as well as in supercell size and shape, respectively. In both plots, there is an apparent split in the Bader charge of Co, with one peak corresponding to 32 atoms with an average Bader charge of 1.27 and the second peak at an average Bader charge of 1.47 for eight atoms. The former charge matches that for the J14 structure without Li and corresponds to the Co^{+2} state. The higher Bader charge corresponds to the Co^{+3} state. The oxidation of some of the Co atoms observed in the DFT is therefore consistent with the XPS data reported by Berardan *et al.*[16,17]

To further quantify and understand the results based on the Bader charges, the spin magnetic moments and the spin resolved DOS projected on the 3*d* orbitals of Co, Cu, and Ni were examined. Plotted in Figure 11 are distributions of Bader charges for the Co, Ni, and Cu ions in the relaxed structure. The shading of each bar denotes the number of cations with a given charge state (as determined from the spin magnetic moments) for the Bader charge. Based on this analysis, as listed in Table II, a total of 10 Co ions oxidized to Co^{+3}, seven with high spin (HS) state and three with intermediate spin (IS) state configurations. The former have

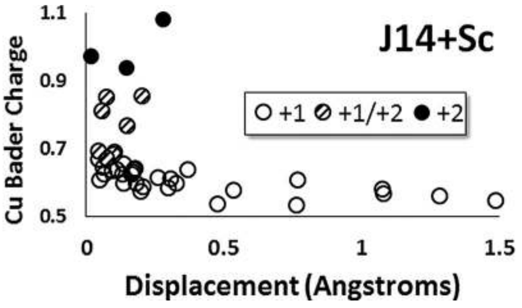

FIG. 9. Bader charge for each of the Cu cations in the J14 + Sc system as a function of displacement of the Cu cation from its ideal lattice site. The formal charges are indicated by the shading.

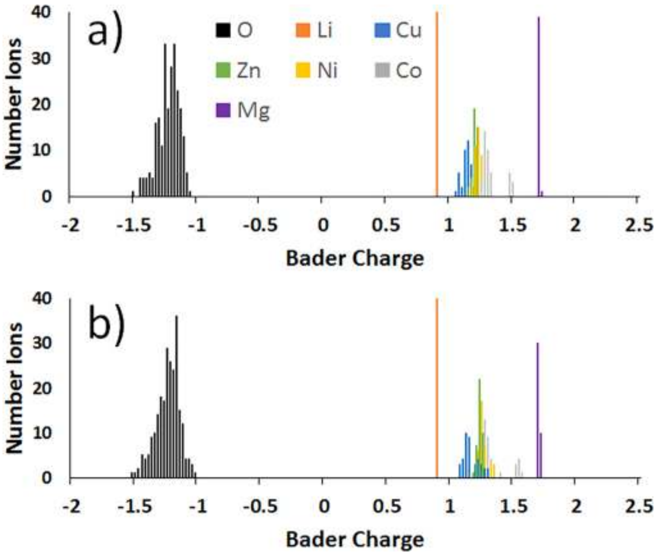

FIG. 10. Bader charge distributions from the DFT calculations. (a) From the 480 atom randomized J14 + I composition on an ideal rock salt lattice. (b) Same system as (a) after relaxation.

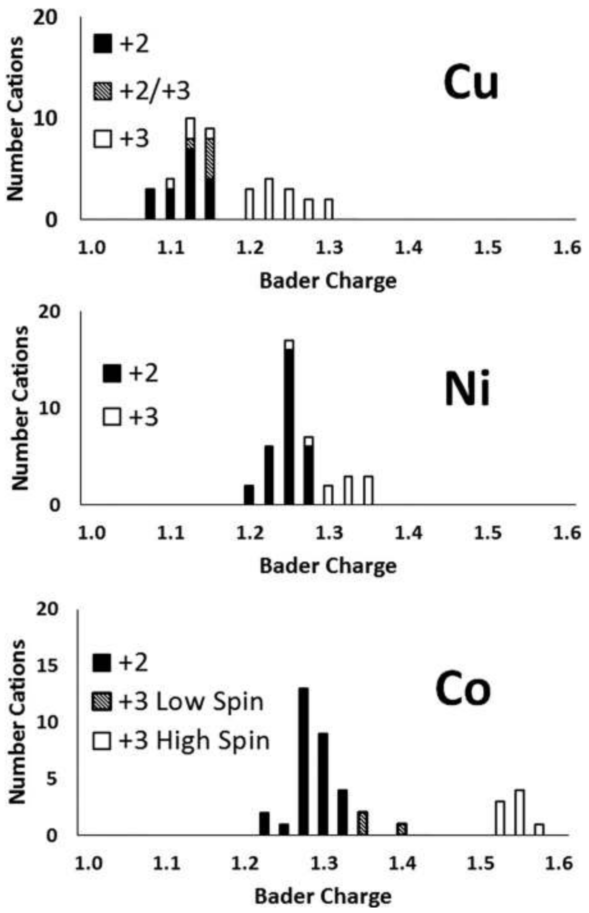

FIG. 11. Bader charge distributions for Cu, Ni, and Co cations in the J14 + Li relaxed system. The shading of each bar denotes the charge state as determined from the spins.

Bader charges that are well-separated from those associated with a +2 formal charge state. The intermediate spin, +3 Co cations have Bader charges that are closer to those associated with the +2 states, but that do not overlap with the +2 Bader charge distribution. A total of 10 Ni cations were identified as having been oxidized to a +3 formal charge state, all of which had a low spin (LS) state. From Figure 11, it is apparent that although the cations identified as having a +3 formal charge state tend to have large Bader charges, there is some overlap in the charge distributions. A total of 17 of the Cu cations were identified as having been oxidized to a +3 formal charge state, a definitive charge state could not be determined for five more Cu cations, and the remaining Cu cations did not change formal charge state. Like the Ni cations, the oxidized Cu cations tend to have large Bader charges, but there is some overlap in the Bader charge distributions associated with the different formal charge states. The origin of this overlap is unclear, although it may be related to the way in which Bader charge is defined from the DFT charge distributions.

From the data presented in Figure 6, oxidation of Co, Ni, and Cu from the introduction of Li into the J14 composition does not result in large changes in the average displacement from the ideal lattice sites for any of the elements. This is in contrast to the data for the addition of Sc, as discussed above. Based on the effective radii plotted in Figure 1, oxidized Co, Ni, and Cu fall well below the region of ionic radii defined by the J14 elements. The DFT calculations, however, suggest that addition of Li can oxidize these elements without the introduction of significant strain as suggested by the data in Figure 6. Together with the relatively large displacements of some of the reduced copper cations in the J14 + Sc composition, this suggests that empirical stability parameters based on ionic radius may be more complicated (or less predictive) than those used for non-oxide MHEAs.[3]

Plotted in Figure 12 are spin polarized DOS projected on the *d*-orbitals of Co, Ni, and Cu. The spin configuration diagrams illustrating the *d*-orbital occupations are also represented in Figure 12. In the case of Co, the identification of +2 and +3 charge states is relatively straightforward. Co^{+2} has a d^7 configuration with all five up-states and two down-states occupied and located below the Fermi energy (E_F), while the remaining three empty down-states are located well above E_F, as illustrated in the upper panel of Figure 12(a). Co^{+3} has six *d* electrons, and it can be in a HS or LS state. The electronic structure of Co^{+3} HS, illustrated in the mid-panel of Figure 12(a), is similar to that of Co^{+2} with the exception that there is only one occupied down-state in Co^{+3} HS. This difference is visible in Figure 12(a), where the occupied spin-down DOS corresponding to Co^{+3} HS (mid-panel) is significantly reduced compared to Co^{+2}. In the LS configuration, Co^{+3} can have one or two empty spin-up states. Based on the calculated spin magnetic moments and Bader charge analysis, in the present case, the LS Co^{+3} has only one empty up-state. This is illustrated in the lower panel of Figure 12(a). Using a similar analysis of the electronic structure, Ni^{+2} (d^8) and Ni^{+3} (d^7) can be identified. As illustrated in the upper panel of Figure 12(b), all spin-up 3*d* states of Ni^{+2} are occupied while in the spin-down channel, the occupied and empty states are well separated. The empty spin-up states located in the vicinity of E_F, illustrated in the lower panel of Figure 12(b), indicate that Ni^{+3} is in a LS configuration. In the case of Cu, the distinction between the +2 and +3 oxidation states is not as clear. The electronic structures of Cu^{+2} (d^9) and Cu^{+3} (d^8) HS are quite similar; both have completely occupied spin-up states with one and two empty spin-down states corresponding to Cu^{+2} and Cu^{+3} HS, respectively. Therefore, distinguishing between Cu^{+2} and Cu^{+3} HS configurations based solely on DOS calculations is not possible. The PDOS calculations, however, indicate that several Cu ions have empty spin-up *d*-states, suggesting that these Cu are probably in the LS + 3 configuration. This is illustrated in the lower panel of Figure 12(c).

These DFT results provide an alternative interpretation of the data presented and discussed by Berardan *et al.* for the addition of Li to J14.[16,17] Rather than needing to invoke oxygen vacancies to explain the changes in lattice constant and the XPS data, it appears that both can be explained by oxidation of a fraction of Co^{+2} to Co^{+3}, as well as oxidation of some of Cu and Ni from +2 to +3. For Co, the *d*-states near the Fermi level are distinct for the two oxidation states, and the Bader charges are well separated according to a spin state. In contrast, the DOS for the Ni and Cu atoms in their respective +2 and +3 charge states are very similar and the

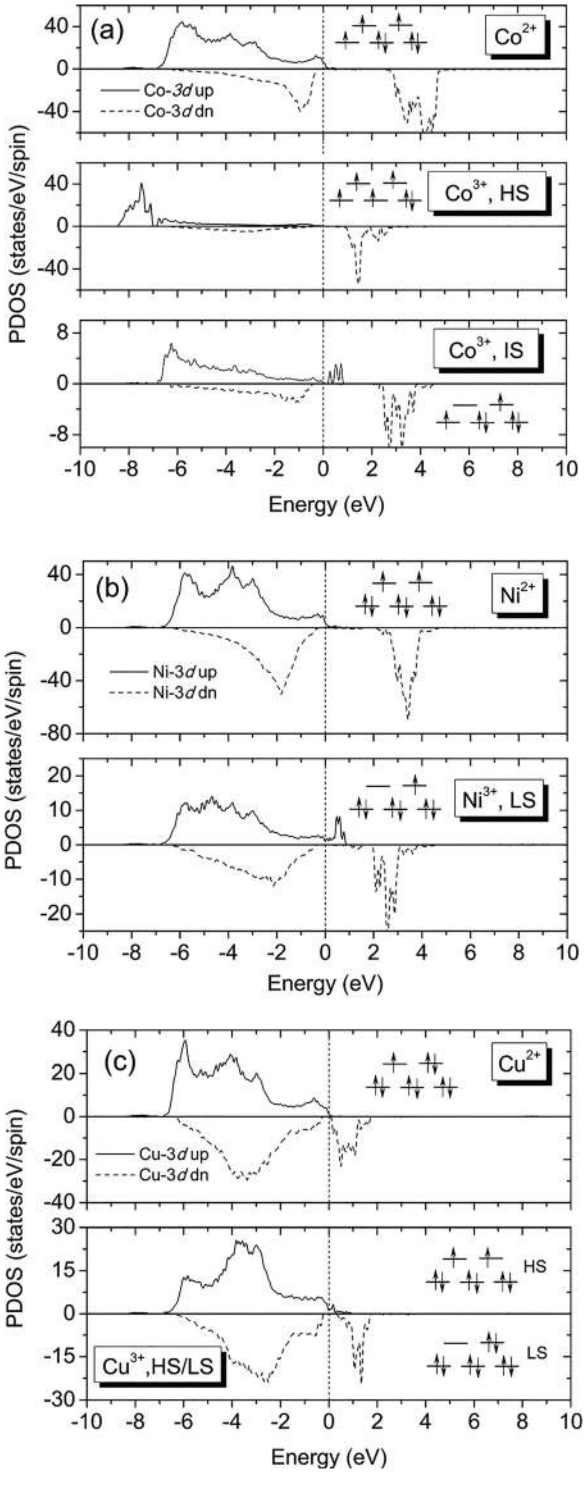

FIG. 12. Partial DOS resolved by spin for the d electrons near the Fermi level for (a) Co, (b) Ni, and (c) Cu in the J14 + Li system.

Bader charges are not well separated by the spin state. Therefore, for this system, it may be difficult to experimentally discern a signature that indicates the two charge states. It is important to note that we are not suggesting that O vacancies are not present and do not play a potential role in the structure and properties of this system, but rather that the experimental data can be interpreted in a way that do not require the assumption of O vacancies.

V. CONCLUSIONS

We have carried out an extensive set of DFT calculations on three entropic oxides, J14, J14 + Li, and J14 + Sc, to explore their properties, to understand the role of charge distribution and electronic states on their structure, and to probe whether simple empirical expressions may exist that could predict the stability of different compositions. For all three structures, our calculations predict that the lattice constants for the random structures can be predicted reasonably well as the average of those for the ternary structures. For J14, the calculations predict that Bader charges for each element are transferable from the binary, ternary, and random structures, suggesting that for this system, it may be possible to develop expressions for ionic bonding in the random structures based on that in the corresponding binary and ternary compositions. A splitting of the Cu *d*-states near the Fermi level after relaxation from an ideal rocksalt structure suggests a Jahn-Teller distortion involving O atom displacement.

For J14 + Sc and J14 + Li, it was found that charge compensation due to the addition of cations with a +3 and +1 formal charge state, respectively, results in significant charge transfer to the other cations. Because of this, the average Bader charges in the entropic structures are not transferable from the respective binary compositions, but they can be estimated from the average values from the ternary compositions. Addition of Sc to J14 results in the reduction of a majority of Cu cations, along with a few Co and Ni cations. The former is associated with large displacements of some of the reduced Cu cations from their ideal lattice sites compared to the other elements. Addition of Li to J14 results in the oxidation of not only some of the Co from a +2 to a +3 state but also oxidation of some of Ni and Cu. In contrast to J14 + Sc, no substantial displacement of the cations from their ideal lattice sites was given by the calculations for the addition of Li to J14. Addition of Li did reduce the lattice constant and the band gap compared to J14, both of which are consistent with experimental studies.[16,17] Also noted is that in the J14 + Li structure, the spin resolved DOS for the d states for Co^{+3} is very different from that for Co^{+2}, and that the corresponding Bader charges are well separated. In contrast, for both Cu and Ni, the two DOS are very similar for the +2 and +3 oxidation states, and the Bader charges form continuous distributions. This result implies that for this system, experimental signatures for the different oxidation states may be challenging to detect for Cu and Ni compared to Co.

Based on the analysis of the DFT results presented here, empirical stability parameters for these entropic oxides may be more complicated than what has been successfully used for non-oxide MHEAs. It has been shown, for example, that atomic radii used in a relatively simple mathematical expression combined with heats of mixing for pairs of constituent elements can lead to relatively accurate predictions of non-oxide MHEAs.[3] An equivalent expression for these entropic oxides would use ionic radii and charges from binary or ternary compositions. It is clear from these calculations that constraints introduced from charge neutrality potentially complicate these considerations. Furthermore, experimental data for a wide range of random oxide compositions needed to validate and develop such expressions are not yet available.

In addition to the insights into bonding in these random oxides, the results reported here have implications for constructing inter-atomic potentials for these systems. Because of the transferability in Bader charges for the J14 composition between binary, ternary, and random structures, it may be possible to achieve reasonable accuracy for many applications assuming fixed charges that are independent of environment. An example of these types of potentials includes the shell model.[33] However, the addition of Sc and Li to the J14 composition apparently introduces environment-dependent charge transfer effects that may have to be included depending on the applications and necessary level of accuracy in the inter-atomic forces.[34]

Finally, there are some caveats that need to be addressed in future studies. For each system, only one large configuration was studied, and this configuration was generated as a representation of a fully random structure via the special quasi-random structure algorithm.[32] There may be effects related to charge transfer and strain that could lead to correlations in cation neighbors that would require further calculations to quantify. We have also not attempted to include oxygen vacancies or interstitial defects in the present calculations. As pointed out previously, the former may play an important role in the structure and properties of these systems.[16,17]

ACKNOWLEDGMENTS

This work was supported by a Multi-Disciplinary University Research Initiative through Award No. N00014-15-1-2863 from the Office of Naval Research and by National Science Foundation Contract No. 1610844.

[1] S. Guo, "Phase selection rules for cast high entropy alloys: An overview," Mater. Sci. Technol. **31**, 1223–1230 (2015).

[2] O. N. Senkov and D. B. Miracle, "A new thermodynamic parameter to predict formation of solid solution or intermetallic phases in high entropy alloys," J. Alloys Compd. **658**, 603–607 (2016).

[3] Y. Zhang, Y. J. Zhou, J. P. Lin, G. L. Chen, and P. K. Liaw, "Solid-solution phase formation rules for multi-component alloys," Adv. Eng. Mater. **10**, 534–538 (2008).

[4] Y. Zhang *et al.*, "Microstructures and properties of high-entropy alloys," Prog. Mater. Sci. **61**, 1–93 (2014).

[5] K. M. Youssef, A. J. Zaddach, C. Niu, D. L. Irving, and C. C. Koch, "A novel low-density, high-hardness, high-entropy alloy with close-packed single-phase nanocrystalline structures," Mater. Res. Lett. **3**, 95–99 (2015).

[6] C. Niu *et al.*, "Spin-driven ordering of Cr in the equiatomic high entropy alloy NiFeCrCo," Appl. Phys. Lett. **106**, 161906 (2015).

[7] M.-H. Tsai and J.-W. Yeh, "High-entropy alloys: A critical review," Mater. Res. Lett. **2**, 107–123 (2014).

[8] J. W. Yeh, Y. L. Chen, S. J. Lin, and S. K. Chen, "High-entropy alloys – A new era of exploitation," Mater. Sci. Forum **560**, 1–9 (2007).

[9] S. J. Mary, R. Nagalakshmi, and R. Epshiba, "High entropy alloys properties and its applications – An overview," Eur. Chem. Bull. **4**, 279–284 (2015).

[10] D. B. Miracle, "Critical assessment 14: High entropy alloys and their development as structural materials," Mater. Sci. Technol. **31**, 1142–1147 (2015).

[11] O. N. Senkov, C. Woodward, and D. B. Miracle, "Microstructure and properties of aluminum-containing refractory high-entropy alloys," JOM **66**, 2030–2042 (2014).

[12] O. N. Senkov, S. V. Senkova, D. B. Miracle, and C. Woodward, "Mechanical properties of low-density, refractory multi-principal element alloys of the Cr–Nb–Ti–V–Zr system," Mater. Sci. Eng. A **565**, 51–62 (2013).

[13] O. N. Senkov, S. V. Senkova, C. Woodward, and D. B. Miracle, "Low-density, refractory multi-principal element alloys of the Cr-Nb-Ti-V-Zr system: Microstructure and phase analysis," Acta Mater. **61**, 1545–1557 (2013).

[14] O. N. Senkov *et al.*, "Oxidation behavior of a refractory $NbCrMo_{0.5}Ta_{0.5}TiZr$ alloy," J. Mater. Sci. **47**, 6522–6534 (2012).

[15] C. M. Rost *et al.*, "Entropy-stabilized oxides," Nat. Commun. **6**, 8485 (2015).

[16] D. Berardan, S. Franger, D. Dragoe, A. K. Meena, and N. Dragoe, "Colossal dielectric constant in high entropy oxides," Phys. Status Solidi RRL **10**, 328–333 (2016).

[17] D. Berardan, S. Franger, A. K. Meena, and N. Dragoe, "Room temperature lithium superionic conductivity in high entropy oxides," J. Mater. Chem. A **4**, 9536–9541 (2016).

[18] C. M. Rost, "Entropically-stabilized oxides: Explorations of a novel class of multicomponent materials," Ph.D. thesis, North Carolina State University, 2016.

[19] M. C. Troparevsky, J. R. Morris, P. R. C. Kent, A. R. Lupini, and G. M. Stocks, "Criteria for predicting the formation of single-phase high-entropy alloys," Phys. Rev. X **5**, 011041 (2015).

[20] M. C. Troparevsky *et al.*, "Beyond atomic sizes and hume-rothery rules: Understanding and predicting high-entropy alloys," JOM **67**, 2350–2363 (2015).

[21] R. Shannon, "Revised effective ionic radii and systematic studies of interatomic distances in halides and chalcogenides," Acta Crystallogr., Sect. A **32**, 751–767 (1976).

[22] N. Kato and A. R. Lang, "A study of Pendellossung fringes in x-ray diffraction," Acta Crystallogr. **12**, 787 (1959).

[23] Q. Shen, *Methods in Materials Research* (John Wiley & Sons, 2000), Vol. 8.

[24] P. E. Blöchl, "Projector augmented-wave method," Phys. Rev. B **50**, 17953–17979 (1994).

[25] G. Kresse and J. Furthmüller, "Efficiency of ab-initio total energy calculations for metals and semiconductors using a plane-wave basis set," Comput. Mater. Sci. **6**, 15–50 (1996).

[26] G. Kresse and J. Furthmüller, "Efficient iterative schemes for *ab initio* total-energy calculations using a plane-wave basis set," Phys. Rev. B: Condens. Matter **54**, 11169–11186 (1996).

[27] G. Kresse and J. Hafner, "*Ab initio* molecular dynamics for liquid metals," Phys. Rev. B **47**, 558–561 (1993).

[28] J. Perdew, K. Burke, and M. Ernzerhof, "Generalized gradient approximation made simple," Phys. Rev. Lett. **77**, 3865–3868 (1996).

[29] S. L. Dudarev, G. A. Botton, S. Y. Savrasov, C. J. Humphreys, and A. P. Sutton, "Electron-energy-loss spectra and the structural stability of nickel oxide: An LSDA + U study," Phys. Rev. B **57**, 1505–1509 (1998).

[30] C. E. Calderon *et al.*, "The AFLOW standard for high-throughput materials science calculations," Comput. Mater. Sci. **108**, 233–238 (2015).

[31] G. Henkelman, A. Arnaldsson, and H. Jónsson, "A fast and robust algorithm for Bader decomposition of charge density," Comput. Mater. Sci. **36**, 354–360 (2006).

[32] A. Zunger, S. Wei, L. Ferreira, and J. Bernard, "Special quasirandom structures," Phys. Rev. Lett. **65**, 353–356 (1990).

[33] G. Jacucci, I. R. McDonald, and K. Singer, "Introduction of the shell model of ionic polarizability into molecular dynamics calculations," Phys. Lett. A **50**, 141–143 (1974).

[34] A. K. Rappé and W. A. Goddard III, "Charge equilibration for molecular dynamics simulations," J. Phys. Chem. **95**, 3358–3363 (1991).